# An element-free Galerkin method for probabilistic mechanics and reliability

S. Rahman [*], B.N. Rao

*College of Engineering, The University of Iowa, 2140 Seamans Center, Iowa City, IA 52242, USA*

## Abstract

A stochastic element-free Galerkin method was developed for reliability analysis of linear-elastic structures with spatially varying random material properties. A random field representing material properties was discretized into a set of random variables with statistical properties obtained from the statistical properties of random field. In conjunction with meshless formulations, the first-order reliability method was employed to predict the full probabilistic characteristics of a structural response. Unlike the stochastic finite element method, the stochastic mesh-free method does not require a structured mesh, instead only a scattered set of nodal points is required in the domain of interest. As well, there is no need for fixed connectivities between nodes. Numerical examples show good agreement between the results of the developed method and Monte Carlo simulation. Furthermore, the stochastic meshless method provides convergent solutions of the probability of failure. Since mesh generation of complex structures can be far more time-consuming and costly effort than solution of a discrete set of equations, the developed meshless method provides an attractive alternative to finite element method for solving stochastic-mechanics problems. © 2001 Elsevier Science Ltd. All rights reserved.

## 1. Introduction

In recent years, much attention has been focused on mesh-free methods, such as smooth particle hydrodynamics (Lucy, 1977; Monaghan, 1988; Libersky et al., 1993), the diffuse element method (Nayroles et al., 1992), the element-free Galerkin method (EFGM) (Belytschko et al., 1994, 1995; Lu et al., 1994; Rao and Rahman, 2000), h–p clouds (Duarte and Oden, 1996), the partition of unity method (Melenk and Babuska, 1996), and the reproducing kernel particle method (Liu et al., 1995, 1997), to solve solid-mechanics problems without using a structured grid. Among these methods, EFGM is particularly appealing, due to its simplicity and a formulation that corresponds to the well-established finite element method

---

[*] Corresponding author. Tel.: +1-319-335-5679; fax: +1-319-335-5669.

*E-mail address:* rahman@engineering.uiowa.edu (S. Rahman).

*URL:* http://www.engineering.uiowa.edu/~rahman.

(FEM). Similar to other meshless methods, EFGM employs recently developed approximation theories that permit the resultant shape functions to be constructed entirely in terms of arbitrarily placed nodes. Since no element connectivity data is needed, burdensome meshing or remeshing required by FEM is avoided. This issue is particularly important when solving mechanics problems characterized by a continuous change in geometry of the domain under analysis. Crack propagation in solids and simulation of manufacturing processes involving large deformation, such as extrusion, molding, metal forming, are prime examples for which standard FEM is ineffective in addressing substantial remeshing or severe mesh distortion. Hence, EFGM and other meshless methods provide an attractive alternative to FEM in solving computational-mechanics problems.

Most development in EFGM and other meshless methods, however, has been focused on deterministic problems. Research in probabilistic modeling using EFGM or other meshless methods has not been widespread and is only currently gaining attention. Recently, Rahman and Rao (2001) and Rahman and Xu (2001) developed several stochastic meshless methods for solving solid-mechanics problems in linear elasticity that involves spatially varying random material properties. In these methods, the material properties were modeled as a homogeneous Gaussian random field. Using spatial discretization of a random field, classical perturbation expansions were derived in conjunction with meshless equations to predict the second-moment characteristics of response (Rahman and Rao, 2001). Subsequently, Rahman and Xu (2001) invoked Karhunen–Loève expansion to parameterize random fields in the development of a Neumann series expansion to conduct second-moment analysis. Similar to stochastic finite element methods (SFEMs) (Vanmarcke and Grigoriu, 1983; Der Kiureghian and Liu, 1986; Liu et al., 1986, 1987; Der Kiureghian and Ke, 1988; Yamazaki and Shinozuka, 1988; Spanos and Ghanem, 1989; Deodatis, 1991; Ghanem and Spanos, 1991; Li and Der Kiureghian, 1992; Zhang and Ellingwood, 1994; IASSAR, 1997), prevalent in the stochastic mechanics community, stochastic meshless methods also provide accurate estimates of the mean and variance of response when random fluctuations in input are small. Although the second-moment properties are quite useful, these methods do not provide any information with respect to the probability distribution of the response, which is vital for evaluating the reliability of structures. As a result, there is considerable interest in developing a stochastic meshless method that is capable of predicting the full probabilistic characteristics of random responses. Consequently, meshless-based methods for reliability analysis presents rich, relatively unexplored area for research in computational stochastic mechanics.

This paper presents a stochastic element-free Galerkin method (SEFGM) for probabilistic analysis of linear-elastic structures that involves random material properties. The material property was modeled as a homogeneous Gaussian random field. Using spatial discretization, the random field was discretized into a set of random variables with statistical properties obtained from the statistical properties of the random field. In conjunction with the EFGM, the first-order reliability method (FORM) was employed to predict the full probabilistic characteristics of the structural response. Numerical examples based on one- and two-dimensional linear-elasticity problems are presented to examine the accuracy and convergence of the proposed method.

## 2. Element-free Galerkin method

### 2.1. Moving least-squares and meshless shape function

Consider a function $u(\boldsymbol{x})$ over a domain $\Omega \subseteq \Re^K$, where $K = 1, 2,$ or 3. Let $\Omega_x \subseteq \Omega$ denote a sub-domain describing the neighborhood of a point $\boldsymbol{x} \in \Re^K$ located in $\Omega$. According to the moving least-squares (MLS) (Lancaster and Salkauskas, 1981) method, the approximation $u^h(\boldsymbol{x})$ of $u(\boldsymbol{x})$ is

$$u^h(\boldsymbol{x}) = \sum_{i=1}^{m} p_i(\boldsymbol{x})a_i(\boldsymbol{x}) = \boldsymbol{p}^{\mathrm{T}}(\boldsymbol{x})\boldsymbol{a}(\boldsymbol{x}), \tag{1}$$

where $\boldsymbol{p}^{\mathrm{T}}(\boldsymbol{x}) = \{p_1(\boldsymbol{x}), p_2(\boldsymbol{x}), \ldots, p_m(\boldsymbol{x})\}$ is a vector of complete basis functions of order $m$ and $\boldsymbol{a}(\boldsymbol{x}) = \{a_1(\boldsymbol{x}), a_2(\boldsymbol{x}), \ldots, a_m(\boldsymbol{x})\}$ is a vector of unknown parameters that depend on $\boldsymbol{x}$. For example, in two dimensions ($K = 2$) with $x_1$- and $x_2$-coordinates,

$$\boldsymbol{p}^{\mathrm{T}}(\boldsymbol{x}) = \{1, x_1, x_2\}, \quad m = 3 \tag{2}$$

and

$$\boldsymbol{p}^{\mathrm{T}}(\boldsymbol{x}) = \{1, x_1, x_2, x_1^2, x_1 x_2, x_2^2\}, \quad m = 6, \tag{3}$$

which represent linear and quadratic basis functions, respectively, and are commonly used in solid mechanics.

In Eq. (1), the coefficient vector $\boldsymbol{a}(\boldsymbol{x})$ is determined by minimizing a weighted discrete $\mathscr{L}_2$ norm, defined as

$$J(\boldsymbol{x}) = \sum_{I=1}^{n} w_I(\boldsymbol{x}) \big[ \boldsymbol{p}^{\mathrm{T}}(\boldsymbol{x}_I)\boldsymbol{a}(\boldsymbol{x}) - d_I \big]^2 = [\boldsymbol{P}\boldsymbol{a}(\boldsymbol{x}) - \boldsymbol{d}]^{\mathrm{T}} \boldsymbol{W} [\boldsymbol{P}\boldsymbol{a}(\boldsymbol{x}) - \boldsymbol{d}], \tag{4}$$

where $\boldsymbol{x}_I$ denotes the coordinates of node $I$, $\boldsymbol{d}^{\mathrm{T}} = \{d_1, d_2, \ldots, d_n\}$ with $d_I$ representing the nodal parameter for node $I$, $\boldsymbol{W} = \mathrm{diag}[w_1(\boldsymbol{x}), w_2(\boldsymbol{x}), \ldots, w_n(\boldsymbol{x})]$ with $w_I(\boldsymbol{x})$ denoting the weight function associated with node $I$ such that $w_I(\boldsymbol{x}) > 0$ for all $\boldsymbol{x}$ in the support $\Omega_{\boldsymbol{x}}$ of $w_I(\boldsymbol{x})$ and zero otherwise, $n$ is the number of nodes in $\Omega_{\boldsymbol{x}}$ for which $w_I(\boldsymbol{x}) > 0$, and

$$\boldsymbol{P} = \begin{bmatrix} \boldsymbol{p}^{\mathrm{T}}(\boldsymbol{x}_1) \\ \boldsymbol{p}^{\mathrm{T}}(\boldsymbol{x}_2) \\ \vdots \\ \boldsymbol{p}^{\mathrm{T}}(\boldsymbol{x}_n) \end{bmatrix} \in \mathscr{L}(\mathfrak{R}^n \times \mathfrak{R}^m). \tag{5}$$

A number of weight functions are available in the literature (Belytschko et al., 1994, 1995; Lu et al., 1994; Liu et al., 1995, 1997; Duarte and Oden, 1996; Melenk and Babuska, 1996; Rao and Rahman, 2000). In this work, a weight function based on the student's $t$-distribution (Rao and Rahman, 2000), which represents the scaled probability density function of a standard Gaussian random variable divided by the square root of a chi-squared random variable with $\beta$ degrees of freedom (Middleton, 1996), was used; it can be expressed as

$$w_I(\boldsymbol{x}) = \begin{cases} \dfrac{\left(1+\beta^2 \frac{z_I^2}{z_{mI}^2}\right)^{-(1+\beta)/2} - (1+\beta^2)^{-(1+\beta)/2}}{1-(1+\beta^2)^{-(1+\beta)/2}}, & z_I \leqslant z_{mI} \\ 0, & z_I > z_{mI} \end{cases}, \tag{6}$$

where $\beta$ is a parameter controlling the shape of the weight function, $z_I = \|\boldsymbol{x} - \boldsymbol{x}_I\|$ is the distance from a sample point $\boldsymbol{x}$ to a node $\boldsymbol{x}_I$, and $z_{mI}$ is the domain of influence of node $I$. The stationarity of $J(\boldsymbol{x})$ with respect to $\boldsymbol{a}(\boldsymbol{x})$ yields

$$\boldsymbol{A}(\boldsymbol{x})\boldsymbol{a}(\boldsymbol{x}) = \boldsymbol{C}(\boldsymbol{x})\boldsymbol{d}, \tag{7}$$

where

$$\boldsymbol{A}(\boldsymbol{x}) = \sum_{I=1}^{n} w_I(\boldsymbol{x})\boldsymbol{p}(\boldsymbol{x}_I)\boldsymbol{p}^{\mathrm{T}}(\boldsymbol{x}_I) = \boldsymbol{P}^{\mathrm{T}}\boldsymbol{W}\boldsymbol{P}, \tag{8}$$

$$C(x) = [w_1(x)p(x_1), \ldots, w_n(x)p(x_n)] = P^T W.$$ (9)

Solving for $a(x)$ in Eq. (7) and then substituting in Eq. (1) yields

$$u^h(x) = \sum_{I=1}^{n} \Phi_I(x)d_I = \Phi^T(x)d,$$ (10)

where

$$\Phi^T(x) = \{\Phi_1(x), \Phi_2(x), \ldots, \Phi_n(x)\} = p^T(x)A^{-1}(x)C(x)$$ (11)

is a vector with its $I$th component,

$$\Phi_I(x) = \sum_{j=1}^{m} p_j(x)[A^{-1}(x)C(x)]_{jI},$$ (12)

representing the shape function of the MLS approximation corresponding to node $I$. The partial derivatives of $\Phi_I(x)$ can also be obtained as

$$\Phi_{I,i}(x) = \sum_{j=1}^{m} \left\{ p_{j,i}(A^{-1}C)_{jI} + p_j(A^{-1}_{,i}C + A^{-1}C_{,i})_{jI} \right\},$$ (13)

where $A^{-1}_{,i} = -A^{-1}A_{,i}A^{-1}$ and $(\ \ )_{,i} = \partial(\ \ )/\partial x_i$.

## 2.2. Variational formulation and discretization

For small displacements in two-dimensional, isotropic, and linear-elastic solids, the equilibrium equations and boundary conditions are

$$\nabla \cdot \sigma + b = 0 \quad \text{in } \Omega$$ (14)

and

$$\sigma \cdot n = \bar{t} \quad \text{on} \quad \Gamma_t \text{ (natural boundary conditions)},$$
$$u = \bar{u} \quad \text{on} \quad \Gamma_u \text{ (essential boundary conditions)},$$ (15)

respectively, where $\sigma = D\epsilon$ is the stress vector, $D$ is the material property matrix, $\epsilon = \nabla_s u$ is the strain vector, $u$ is the displacement vector, $b$ is the body force vector, $\bar{t}$ and $\bar{u}$ are the vectors of prescribed surface tractions and displacements, respectively, $n$ is a unit normal to domain, $\Omega$, $\Gamma_t$ and $\Gamma_u$ are the portions of boundary $\Gamma$ where tractions and displacements are respectively prescribed, $\nabla^T = \{\partial/\partial x_1, \partial/\partial x_2\}$ is the vector of gradient operators, and $\nabla_s u$ is the symmetric part of $\nabla u$. The variational or weak form of Eqs. (14) and (15) is

$$\int_\Omega \sigma^T \delta\epsilon \, d\Omega - \int_\Omega b^T \delta u \, d\Omega - \int_{\Gamma_t} \bar{t}^T \delta u \, d\Gamma - \delta W_u = 0,$$ (16)

where $\delta$ denotes the variation operator and $\delta W_u$ represents a term that enforces essential boundary conditions. The explicit form of this term depends on the method by which the essential boundary conditions are imposed (Belytschko et al., 1994, 1995; Lu et al., 1994; Rao and Rahman, 2000). In this study, $W_u$ is defined as

$$W_u = \sum_{x_J \in \Gamma_u} f^T(x_J)[u(x_J) - \bar{u}(x_J)],$$ (17)

where $f^T(x_J)$ is the vector of reaction forces at the constrained node $J \in \Gamma_u$. Hence,

$$\delta W_u = \sum_{x_J \in \Gamma_u} \delta f^T(x_J)[u(x_J) - \bar{u}(x_J)] + f^T(x_J)\, \delta u(x_J).$$ (18)

Consider a single boundary constraint, $\bar{u}_i(\boldsymbol{x}_J) = g_i(\boldsymbol{x}_J)$ applied at node $J$ in the direction of the $x_i$ coordinate. The variational form given by Eqs. (16) and (18) can then be expressed by

$$\int_\Omega \boldsymbol{\sigma}^{\mathrm{T}} \delta\boldsymbol{\epsilon}\,\mathrm{d}\Omega + f_i(\boldsymbol{x}_J)\,\delta u_i(\boldsymbol{x}_J) = \int_\Omega \boldsymbol{b}^{\mathrm{T}}\delta\boldsymbol{u}\,\mathrm{d}\Omega + \int_{\Gamma_t} \bar{\boldsymbol{t}}^{\mathrm{T}}\delta\boldsymbol{u}\,\mathrm{d}\Gamma, \tag{19}$$

$$\delta f_i(\boldsymbol{x}_J)[u_i(\boldsymbol{x}_J) - g_i(\boldsymbol{x}_J)] = 0, \tag{20}$$

where $f_i(\boldsymbol{x}_J)$ and $u_i(\boldsymbol{x}_J)$ are the $i$th component of $\boldsymbol{f}(\boldsymbol{x}_J)$ and $\boldsymbol{u}(\boldsymbol{x}_J)$, respectively. From Eq. (10), the MLS approximation of $u_i(\boldsymbol{x}_J)$ is

$$u_i^h(\boldsymbol{x}_J) = \sum_{I=1}^N \Phi_I(\boldsymbol{x}_J)d_I^i = \boldsymbol{\Phi}_J^{i^T}\boldsymbol{d}, \tag{21}$$

where

$$\boldsymbol{\Phi}_J^{i^T} = \begin{cases} \{\Phi_1(\boldsymbol{x}_J), 0, \Phi_2(\boldsymbol{x}_J), 0, \ldots, \Phi_N(\boldsymbol{x}_J), 0\}, & \text{when } i = 1 \\ \{0, \Phi_1(\boldsymbol{x}_J), 0, \Phi_2(\boldsymbol{x}_J), \ldots, 0, \Phi_N(\boldsymbol{x}_J)\}, & \text{when } i = 2 \end{cases}, \tag{22}$$

$$\boldsymbol{d} = \begin{Bmatrix} d_1^1 \\ d_1^2 \\ d_2^1 \\ d_2^2 \\ \vdots \\ d_N^1 \\ d_N^2 \end{Bmatrix} \tag{23}$$

is the vector of nodal parameters or generalized displacements, and $N$ is the total number of nodal points in $\Omega$. Applying Eqs. (21)–(23) in the discretization of Eqs. (19) and (20) yields (Belytschko et al., 1994, 1995; Lu et al., 1994; Rao and Rahman, 2000)

$$\begin{bmatrix} \boldsymbol{k} & \boldsymbol{\Phi}_J^i \\ \boldsymbol{\Phi}_J^{i^T} & 0 \end{bmatrix} \begin{Bmatrix} \boldsymbol{d} \\ f_i(\boldsymbol{x}_J) \end{Bmatrix} = \begin{Bmatrix} \boldsymbol{f}^{\text{ext}} \\ g_i(\boldsymbol{x}_J) \end{Bmatrix}, \tag{24}$$

where

$$\boldsymbol{k} = \begin{bmatrix} \boldsymbol{k}_{11} & \boldsymbol{k}_{12} & \cdots & \boldsymbol{k}_{1N} \\ \boldsymbol{k}_{21} & \boldsymbol{k}_{22} & \cdots & \boldsymbol{k}_{2N} \\ \vdots & \vdots & \vdots & \vdots \\ \boldsymbol{k}_{N1} & \boldsymbol{k}_{N2} & \cdots & \boldsymbol{k}_{NN} \end{bmatrix} \in \mathscr{L}\left(\mathfrak{R}^{2N} \times \mathfrak{R}^{2N}\right) \tag{25}$$

is the stiffness matrix with

$$\boldsymbol{k}_{IJ} = \int_\Omega \boldsymbol{B}_I^{\mathrm{T}}\boldsymbol{D}\boldsymbol{B}_J\,\mathrm{d}\Omega \in \mathscr{L}\left(\mathfrak{R}^2 \times \mathfrak{R}^2\right), \tag{26}$$

representing the contributions of the $J$th node at node $I$,

$$\boldsymbol{f}^{\text{ext}} = \begin{Bmatrix} \boldsymbol{f}_1^{\text{ext}} \\ \boldsymbol{f}_2^{\text{ext}} \\ \vdots \\ \boldsymbol{f}_N^{\text{ext}} \end{Bmatrix} \in \mathfrak{R}^{2N} \tag{27}$$

is the force vector with

$$\boldsymbol{f}_I^{\text{ext}} = \int_\Omega \boldsymbol{\Phi}_I \boldsymbol{b}^{\mathrm{T}} \, \mathrm{d}\Omega + \int_{\Gamma_t} \boldsymbol{\Phi}_I \bar{\boldsymbol{t}}^{\mathrm{T}} \, \mathrm{d}\Gamma \in \mathfrak{R}^2,$$

(28)

$$\boldsymbol{B}_I = \begin{bmatrix} \boldsymbol{\Phi}_{I,1} & 0 \\ 0 & \boldsymbol{\Phi}_{I,2} \\ \boldsymbol{\Phi}_{I,2} & \boldsymbol{\Phi}_{I,1} \end{bmatrix}$$

(29)

and

$$\boldsymbol{D} = \begin{cases} \dfrac{E}{1-v^2} \begin{bmatrix} 1 & v & 0 \\ v & 1 & 0 \\ 0 & 0 & \frac{1-v}{2} \end{bmatrix}, & \text{for plane stress,} \\[2em] \dfrac{E}{(1+v)(1-2v)} \begin{bmatrix} 1-v & v & 0 \\ v & 1-v & 0 \\ 0 & 0 & \frac{1-2v}{2} \end{bmatrix}, & \text{for plane strain} \end{cases}$$

(30)

is the elasticity matrix with $E$ and $v$ representing the elastic modulus and Poisson's ratio, respectively. To perform numerical integration in Eqs. (26) and (28), a background mesh is required, which can be independent of the arrangement of the meshless nodes. However, in this study, the nodes of the background mesh were chosen to coincide with the meshless nodes. Standard Gaussian quadratures were used to evaluate the integrals for assembling the stiffness matrix and the force vector. In general, a $4 \times 4$ quadrature is adequate, except in the cells surrounding a high stress gradient (e.g., near a crack tip) where a $8 \times 8$ quadrature is suggested.

In solving for $\boldsymbol{d}$, the essential boundary conditions must be enforced. The lack of Kronecker delta properties in the meshless shape functions presents some difficulty in imposing the essential boundary conditions in EFGM. Nevertheless, several methods are currently available for enforcing essential boundary conditions. A full transformation method (Rao and Rahman, 2000; Chen and Wang, 2000) was used for the stochastic mechanics applications in this work.

It should be noted that the generalized displacement vector $\boldsymbol{d}$ represents the nodal parameters—not the actual displacements at the meshless nodes. Let

$$\hat{\boldsymbol{d}} = \begin{Bmatrix} u_1^h(\boldsymbol{x}_1) \\ u_2^h(\boldsymbol{x}_1) \\ u_1^h(\boldsymbol{x}_2) \\ u_2^h(\boldsymbol{x}_2) \\ \vdots \\ u_1^h(\boldsymbol{x}_N) \\ u_2^h(\boldsymbol{x}_N) \end{Bmatrix} \in \mathfrak{R}^{2N}$$

(31)

represent the vector of nodal displacements. From Eq. (10),

$$\hat{\boldsymbol{d}} = \boldsymbol{\Lambda} \boldsymbol{d},$$

(32)

where

$$\boldsymbol{\Lambda} = \begin{bmatrix} \boldsymbol{\Phi}_1^{1^T} \\ \boldsymbol{\Phi}_1^{2^T} \\ \boldsymbol{\Phi}_2^{1^T} \\ \boldsymbol{\Phi}_2^{2^T} \\ \vdots \\ \boldsymbol{\Phi}_N^{1^T} \\ \boldsymbol{\Phi}_N^{2^T} \end{bmatrix} \in \mathscr{L}\left(\Re^{2N} \times \Re^{2N}\right) \tag{33}$$

is the transformation matrix. Hence, $\hat{\boldsymbol{d}}$ can be easily calculated when $\boldsymbol{d}$ is known.

## 3. Random field and discretization

### 3.1. Random field

The spatial variability of a material property, such as the elastic modulus $E(\boldsymbol{x})$, can be modeled as a homogeneous random field. Let

$$E(\boldsymbol{x}) = \mu_E[1 + \alpha(\boldsymbol{x})], \tag{34}$$

where $\mu_E = \mathscr{E}[E(\boldsymbol{x})] \neq 0$ is the mean of the elastic modulus that is independent of $\boldsymbol{x}$, and $\alpha(\boldsymbol{x})$ is a zero-mean, scalar, homogeneous random field with its auto-covariance function

$$\Gamma_\alpha(\boldsymbol{\xi}) = \mathscr{E}[\alpha(\boldsymbol{x})\alpha(\boldsymbol{x} + \boldsymbol{\xi})] = \frac{1}{\mu_E^2}\Gamma_E(\boldsymbol{\xi}), \tag{35}$$

where $\Gamma_E(\boldsymbol{\xi})$ is the auto-covariance function of $E(\boldsymbol{x})$, $\boldsymbol{\xi}$ is the separation vector between two points, $\boldsymbol{x} \in \Re^K$ and $\boldsymbol{x} + \boldsymbol{\xi} \in \Re^K$ both located in $\Omega \subseteq \Re^K$, and $\mathscr{E}[\cdot]$ is the expectation operator. In SFEM or meshless applications, it is necessary to discretize a continuous-parameter random field (e.g., Eq. (34)) into a vector of random variables, as described in the following section.

### 3.2. Spatial discretization

For discretization of random fields, various methods, such as the Karhunen–Loève expansion (Ghanem and Spanos, 1991; Spanos and Ghanem, 1989), the midpoint method (Der Kiureghain and Liu, 1986), the local averaging method (Vanmarcke and Grigoriu, 1983), the shape function method (Liu et al., 1986, 1987), the weighted integral method (Deodatis, 1991), and the optimal linear estimation method (Li and Der Kiureghian, 1992) have been developed. The accuracy and convergence of stochastic response due to these discretizations (except the Karhunen–Loève expansion) depend on the size of the finite elements in comparisons with the correlation distance of the random field. In the stochastic meshless method, there are no elements, hence, the discretization effort is not tied to any elements or nodes. For example, consider a discretization of a random field by $M$ number of random variables associated with $M$ discrete points in the structural domain. The value of $M$ and the distribution of these points depend on the correlation distance of $\alpha(\boldsymbol{x})$. It is not necessary that these points coincide with the meshless nodes, as shown in Fig. 1. Hence a large value of $M$, if required for some correlation distance, does not necessarily increase the size of the linear equations for meshless discretization of the domain. This is in contrast to some SFEMs, where the correlation distance of a random field can place serious limitations on the size of the finite elements.
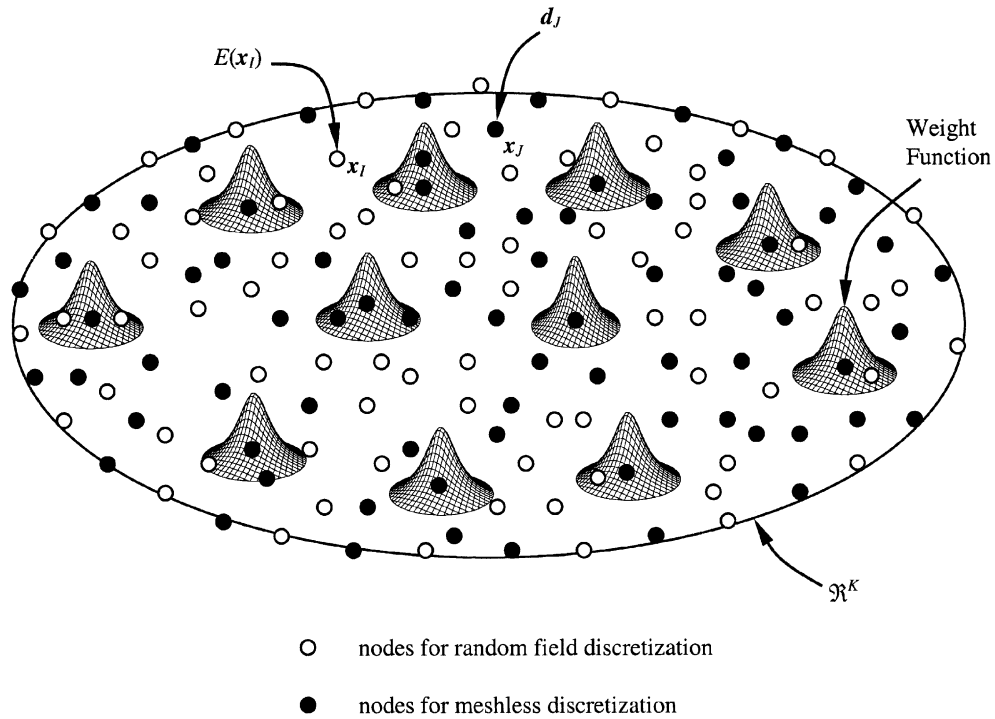
Fig. 1. Meshless and random field discretizations.

Let $\boldsymbol{Y} = \{Y_1, Y_2, \ldots, Y_M\}^{\mathrm{T}}$ denote an $M$-dimensional random vector that adequately represents the random field $\alpha(\boldsymbol{x})$ described earlier. The mean vector $\boldsymbol{\mu} = \mathscr{E}[\boldsymbol{Y}]$ and the covariance matrix $\boldsymbol{\gamma} = \mathscr{E}[(\boldsymbol{Y} - \boldsymbol{\mu})(\boldsymbol{Y} - \boldsymbol{\mu})^{\mathrm{T}}]$ are

$$\boldsymbol{\mu} = \boldsymbol{0}, \tag{36}$$

$$\boldsymbol{\gamma} = \left[\Gamma_\alpha(\boldsymbol{\xi}_{ij})\right], \tag{37}$$

where $\boldsymbol{\xi}_{ij} = \boldsymbol{x}_j - \boldsymbol{x}_i$ is the separation vector between $\boldsymbol{x}_i$ and $\boldsymbol{x}_j$ representing the coordinates of nodes $i$ and $j$, respectively. Hence, the second-moment characteristics of $\boldsymbol{Y}$ can be defined from the knowledge of the mean and covariance function of $\alpha(\boldsymbol{x})$. Note, if $\alpha(\boldsymbol{x})$ is Gaussian, so is the random vector $\boldsymbol{Y}$.

Since $\alpha(\boldsymbol{x})$ or $E(\boldsymbol{x})$ is random field, the elasticity matrix $\boldsymbol{D}(\boldsymbol{x})$ is spatially distributed. When calculating the stiffness matrix (see Eq. (26)) by Gauss quadrature, the values of $\boldsymbol{D}(\boldsymbol{x})$ at Gauss points are required. In this work, the values of $\boldsymbol{Y}$ and meshless shape functions were used to approximate $\boldsymbol{D}(\boldsymbol{x})$ at Gauss points.

## 4. Structural reliability analysis

### 4.1. Random parameters and random response

Given the discretization of the random field by the random vector $\boldsymbol{Y} \in \mathfrak{R}^M$, let $\boldsymbol{K}(\boldsymbol{Y})$ and $\boldsymbol{d}(\boldsymbol{Y})$ denote, respectively, the stiffness matrix and generalized displacement vector, that depend on $\boldsymbol{Y}$ and let $\boldsymbol{F}$ denote the load vector. The discrete meshless equation for the stochastic system is

$$K(Y)d(Y) = F. \tag{38}$$

Inverting Eq. (38),

$$d(Y) = K(Y)^{-1}F \tag{39}$$

and hence, the actual displacement vector, $\hat{d}(Y)$ is

$$\hat{d}(Y) = \Lambda K(Y)^{-1}F. \tag{40}$$

Let $\hat{d}_i^J(Y)$ be the $[2(J-1) + i]$th component of $\hat{d}(Y)$, representing the displacement $[u_i^h(x_J)]$ of node $J$ in the $i$th direction. Suppose the structure fails when $\hat{d}_i^J(Y) > d_0$, where $d_0$ is a deterministic threshold of the displacement. This requirement cannot be satisfied with certainty, since $\hat{d}_i^J(Y)$ depends on the random input vector $Y$. As a result, the performance of the structure should be evaluated using the probability of failure $P_F$, defined as

$$P_F \overset{\text{def}}{=} Pr[g(Y) < 0] \overset{\text{def}}{=} \int_{g(y)<0} f_Y(y)\,\mathrm{d}y, \tag{41}$$

where $f_Y(y)$ is the joint probability density function of $Y$, and $g(y)$ is the performance function given by

$$g(y) = d_0 - \hat{d}_i^J(y). \tag{42}$$

A similar performance function, based on stress and associated failure probability, can also be defined. Regardless of the performance function, the generic expression for the failure probability (Eq. (41)) involves a multi-dimensional probability integration for its evaluation. In this study, the FORM (Madsen et al., 1986) was used to compute this probability. It is briefly described here assuming a generic $M$-dimensional random vector $Y$ and the displacement-based performance function $g(y)$ (Eq. (42)) to calculate the probability of failure defined by Eq. (41).

## 4.2. First-order reliability method

The FORM is based on linear (first-order) approximation of the limit state surface $g(y) = 0$ tangent to the closest point of the surface to the origin of the space. The determination of this point involves nonlinear constrained optimization and is usually performed in the standard Gaussian image $u$ of the original space $y$. The FORM algorithm involves several steps. First, the space $y$ of uncertain parameters $Y$ is transformed into a new $M$-dimensional space $u$ of independent standard Gaussian variables $U$. The original limit state $g(y) = 0$ then is mapped into the new limit state $g_U(u) = 0$ in the $u$ space. Second, the point on the limit state $g_U(u) = 0$ having the shortest distance to the origin of the $u$ space is determined using an appropriate nonlinear optimization algorithm. This point is referred to as the design point, or beta point, and has a distance $\beta_{HL}$ (known as reliability index) to the origin of the $u$ space. Third, the limit state $g_U(u) = 0$ is approximated by a hyperplane $g_L(u) = 0$ tangent to it at the design point. The probability of failure $P_F$ (Eq. (41)) is thus approximated by $P_{F,1} = \Pr[g_L(U) < 0]$ in FORM and is given by (Madsen et al., 1986)

$$P_{F,1} = \Phi(-\beta_{HL}), \tag{43}$$

where

$$\Phi(u) = \frac{1}{\sqrt{2\pi}} \int_{-\infty}^{u} \exp\left(-\frac{1}{2}\xi^2\right) \mathrm{d}\xi \tag{44}$$

is the cumulative distribution function of a standard Gaussian random variable. In this study, the EFGM applied in conjunction with FORM is denoted as the SEFGM. In developing the SEFGM, a recursive quadratic programming algorithm (Lim and Arora, 1986; Arora, 1989) was used to solve the associated

optimization problem. The first-order sensitivities required by this algorithm were calculated analytically and are described in the following section.

### 4.3. Analytical gradients

Most optimization algorithms for solving nonlinear programming problem in FORM require calculation of the gradients of the objective and constraint functions. Using a brute-force finite-difference method to calculate these gradients is often computationally expensive, since many repetitions of deterministic meshless analysis are needed, particularly when there are a large number of random parameters. Consequently, it is useful to calculate the gradients analytically.

In $\boldsymbol{u}$ space, the objective function is quadratic; hence, calculating its first-order derivative with respect to $u_k$, $k = 1, 2, \ldots, M$ is quite trivial. For the constraint function, i.e., the performance function, one must also calculate its derivative with respect to $u_k$. Assume that a transformation of $\boldsymbol{Y} \in \mathfrak{R}^M$ to $\boldsymbol{U} \in \mathfrak{R}^M$, given by

$$\boldsymbol{Y} = \boldsymbol{Y}(\boldsymbol{U}) \tag{45}$$

exists. The performance function in the $\boldsymbol{u}$ space can be written as

$$g_U(\boldsymbol{u}) = d_0 - \hat{d}_i^J(\boldsymbol{y}(\boldsymbol{u})). \tag{46}$$

The first-order derivative of $g_U(\boldsymbol{u})$ with respect to $u_k$ is

$$\frac{\partial g_U(\boldsymbol{u})}{\partial u_k} = -\frac{\partial \hat{d}_i^J(\boldsymbol{y}(\boldsymbol{u}))}{\partial u_k} = -\boldsymbol{\Lambda} \frac{\partial d_i^J(\boldsymbol{y}(\boldsymbol{u}))}{\partial u_k}. \tag{47}$$

Using the chain rule of differentiation,

$$\frac{\partial \boldsymbol{d}}{\partial u_k} = \sum_{j=1}^{M} \frac{\partial \boldsymbol{d}}{\partial y_j} \frac{\partial y_j}{\partial u_k} = \sum_{j=1}^{M} \frac{\partial \boldsymbol{d}}{\partial y_j} R_{jk}, \tag{48}$$

where $R_{jk} = \partial y_j / \partial u_k$, which can be obtained from the explicit form of Eq. (45). Taking the partial derivative of Eq. (38) with respect to $y_j$ yields

$$\frac{\partial \boldsymbol{d}}{\partial y_j} = -\boldsymbol{K}^{-1} \left[ \frac{\partial \boldsymbol{K}}{\partial y_j} \boldsymbol{d} \right]. \tag{49}$$

Then,

$$\frac{\partial \boldsymbol{d}}{\partial u_k} = -\boldsymbol{K}^{-1} \sum_{j=1}^{M} \frac{\partial \boldsymbol{K}}{\partial y_j} \boldsymbol{d} R_{jk}. \tag{50}$$

For a given $\boldsymbol{y}$, the corresponding values of $\boldsymbol{d}$, $\boldsymbol{K}^{-1}$, and $\partial \boldsymbol{K}/\partial y_j$, calculated from the meshless formulation, can be substituted in Eq. (50) to obtain $\partial \boldsymbol{d}/\partial u_k$. Note that $\partial d_i^J/\partial u_k$ is the $[2(J-1)+i]$th component of $\partial \boldsymbol{d}/\partial u_k$. Using Eqs. (47) and (50), the gradients of $g_U(\boldsymbol{u})$ can be evaluated analytically.

Note that when $\alpha(\boldsymbol{x})$ is Gaussian, $\boldsymbol{Y}$ is Gaussian with mean $\boldsymbol{0}$ and covariance matrix $\gamma$. Using the rotational transformation

$$\boldsymbol{Y} = \boldsymbol{Q}\boldsymbol{U} \tag{51}$$

with $\boldsymbol{Q}$ representing the transformation matrix, it is easy to show that

$$\boldsymbol{Q}\boldsymbol{Q}^{\mathrm{T}} = \gamma. \tag{52}$$

In Eq. (52), $\boldsymbol{Q}$ is the Cholesky decomposition of $\gamma$, which can be easily calculated from standard methods of linear algebra. Furthermore, $R_{jk} = Q_{jk}$, where $Q_{jk}$ is the $jk$th element of $\boldsymbol{Q}$. Hence, Eq. (50) becomes

$$\frac{\partial \boldsymbol{d}}{\partial u_k} = -\boldsymbol{K}^{-1} \sum_{j=1}^{M} \frac{\partial \boldsymbol{K}}{\partial y_j} \boldsymbol{d} Q_{jk}. \tag{53}$$

If $\alpha(\boldsymbol{x})$ or $\boldsymbol{Y}$ is Gaussian, Eqs. (47) and (53) provide the analytical gradients of $g_U(\boldsymbol{u})$.

## 5. Numerical examples

Two numerical examples based on one- and two-dimensional problems are presented. In these examples, $\alpha(\boldsymbol{x})$ was modeled as a homogeneous Gaussian random field to describe the random modulus of elasticity $E(\boldsymbol{x})$. For simplicity, the random field was discretized spatially at the same meshless nodes (i.e., $M = N$). The Gaussian assumption implies that there is a non-zero probability of $E(\boldsymbol{x})$ taking on a negative value. To avoid this difficulty, the variance of input random field was confined to a small value. Alternative representations involving truncated Gaussian distribution or other distributions suitable for non-negative random field have been used by various researchers (IASSAR, 1997). These representations were not explored here, because the focus of this study was stochastic meshless analysis. A linear basis function was used in all meshless calculations. For the weight function, a value of $\beta = 2$ was selected. Both first-order reliability and simulation methods were used to calculate various response probabilities of interest.

### 5.1. Example 1: bar with linear body force

Consider a bar AB of length $L = 1$ unit, which is subjected to a linear body force distribution $p(x) = x$ in the $x$ direction, as shown in Fig. 2(a). Point A of the bar is fixed and point B is free. The bar has a constant cross-sectional area $A = 1$ unit. The modulus of elasticity $E(x) = \mu_E[1 + \alpha(x)]$ is random with mean $\mu_E = 1$ unit, and $\alpha(x)$ is a homogeneous Gaussian random field with mean zero and auto-covariance function

$$\Gamma_\alpha(\xi) = \mathscr{E}[\alpha(x)\alpha(x + \xi)] = \sigma_E^2 \exp\left(-\frac{|\xi|}{bL}\right), \tag{54}$$

where $x$ and $x + \xi$ are the co-ordinates of two points in the bar, $\sigma_E$ is the standard deviation of $\alpha(x)$ or $E(x)$, and $b$ is the correlation length parameter. Values of $\sigma_E = 0.1$, $0.2$, and $0.3$ units and $b = 1$ were used for
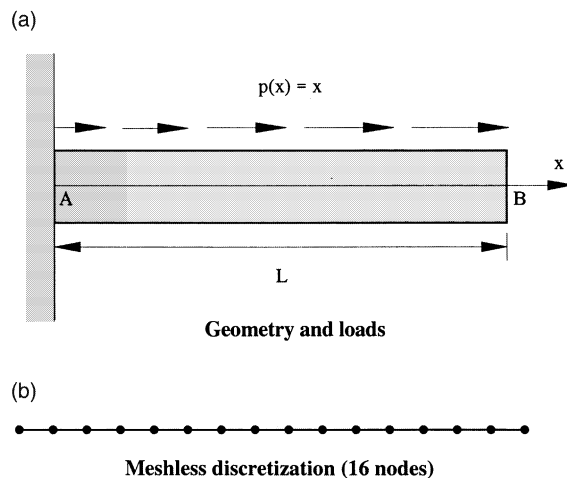


Fig. 2. A bar subjected to linear body force distribution: (a) geometry and loads; (b) meshless discretization (16 nodes).
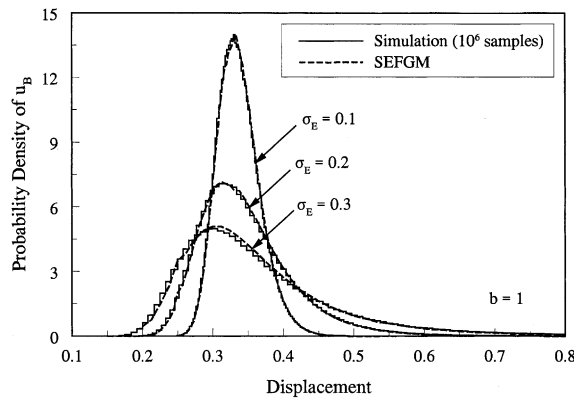
Fig. 3. Probability density function of end displacement of the bar.

numerical calculations. A meshless discretization involving 16 uniformly spaced nodes is shown in Fig. 2(b). A background mesh with its nodes coincident with the meshless nodes was used. The numerical integration involved four-point Gauss quadrature.

The SEFGM developed in this study was applied to determine the full probabilistic characteristics of the axial displacement $u_B(Y)$ at the free end (point B) of the bar. Fig. 3 shows the probability density functions of $u_B(Y)$ for $\sigma_E = 0.1$, 0.2, and 0.3 units, determined by repeating SEFGM analyses to calculate $Pr[u_B(Y) \leqslant u_0]$ and then taking the numerical derivative with respect to $u_0$. Corresponding histograms from Monte Carlo simulation, involving $10^6$ realizations of $u_B(Y)$ by meshless method, are also shown in Fig. 3. The probability densities by SEFGM agree very well with the histograms. Fig. 4 shows how the probability of failure $Pr[u_B(Y) > u_0]$ varies as a function of $u_0$ for all three values of $\sigma_E$. Both the SEFGM and simulation method ($10^6$ samples) were used to generate these plots. The failure probability increases with $\sigma_E$ as expected. The developed SEFGM using FORM provides accurate estimates of the failure probability of the bar when compared with the simulation results.

To study the convergence properties of the failure probability, additional stochastic meshless analyses were performed by increasing the number of nodes ($N$) from 2 to 26. For each value of $N$, a uniform spacing was used for meshless discretization of the bar. Also, the values of $b = 1$ and $\sigma_E = 0.1$ units were used for
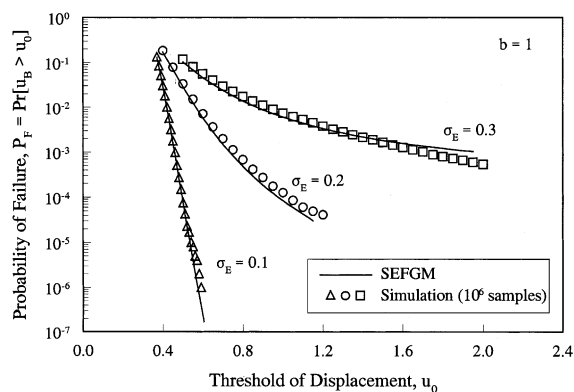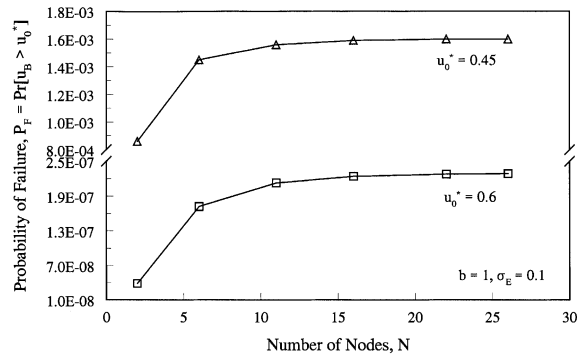


Fig. 4. Probability of failure of the bar.

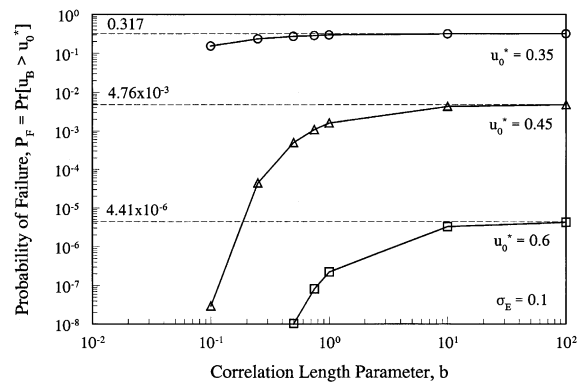Fig. 5. Convergence of failure probability.



Fig. 6. Effect of correlation length on failure probability of the bar.

each analysis. Fig. 5 shows the predicted probability of failure $Pr[u_B(\mathbf{Y}) > u_0^*]$ for $u_0^* = 0.45$ and 0.6 units as a function of $N$. As can be seen, SEFGM produces convergent solutions of the probability of failure.

Fig. 6 plots $Pr[u_B(\mathbf{Y}) > u_0^*]$ for $\sigma_E = 0.1$ units and $u_0^* = 0.35$, 0.45, and 0.6 units when the correlation length parameter $b$ is varied from 0.1 to 100. The results in Fig. 6, calculated using SEFGM, indicate that the upper bound of the failure probability occurs when $b \to \infty$, i.e., when $\mathbf{Y}$ is perfectly correlated. Note, in this case, the random field $E(x)$ degenerates to a random variable $E$ (say). Hence, the axial displacement of the bar at point B can be determined analytically as $u_B = 1/(3E)$. Using this analytical solution and $\sigma_E = 0.1$ units, the exact failure probabilities for $u_0^* = 0.35$, 0.45, and 0.6 units are 0.317, $4.76 \times 10^{-3}$, and $4.41 \times 10^{-6}$, respectively. These exact solutions match with the SEFGM solutions in Fig. 6 when $b \to \infty$.

## 5.2. Example 2: square plate under tension

Consider a square plate as shown in Fig. 7(a). The plate has dimension $L = 1$ unit and is subjected to a uniformly distributed load of magnitude $p = 1$ unit. The square domain of the plate was discretized by 49 nodes equally spaced, as shown in Fig. 7(b). The Poisson's ratio $v$ of 0.3 was selected. The modulus of elasticity $E(\mathbf{x})$ was represented by $E(\mathbf{x}) = \mu_E[1 + \alpha(\mathbf{x})]$, where $\mu_E = 1$ unit is the constant mean over the domain and $\alpha(\mathbf{x})$ is a homogeneous Gaussian random field with mean zero and auto-covariance function

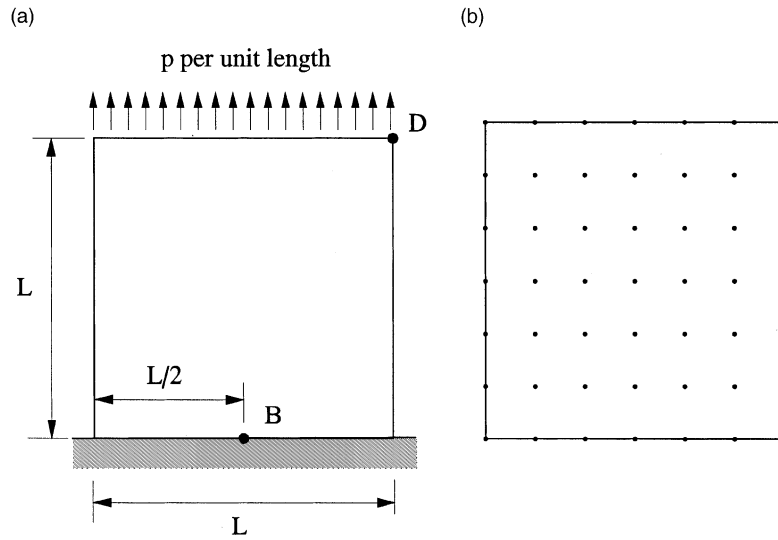(a)                                                          (b)



Fig. 7. A square plate subjected to uniformly distributed tension: (a) geometry and loads; (b) meshless discretization (49 nodes).

$$\Gamma_\alpha(\boldsymbol{\xi}) = \mathscr{E}[\alpha(\boldsymbol{x})\alpha(\boldsymbol{x}+\boldsymbol{\xi})] = \sigma_E^2 \exp\left[-\left(\frac{|\xi_1|}{b_1 L} + \frac{|\xi_2|}{b_2 L}\right)\right], \tag{55}$$

where $\boldsymbol{x} \equiv (x_1, x_2)$ and $\boldsymbol{x} + \boldsymbol{\xi} \equiv (x_1 + \xi_1, x_2 + \xi_2)$ are the co-ordinates of two points in the plate, $\sigma_E = 0.12$ and 0.24 units, and the correlation length parameters are $b_1 = 1$, and $b_2 = 2$. The background mesh was chosen such that its nodes coincide with the meshless nodes. An $8 \times 8$ Gauss quadrature rule was used for all cells.

Fig. 7(a) also shows the locations of two points B and D in the plate. Let $u_2^D(\boldsymbol{Y})$ and $\sigma_{22}^B(\boldsymbol{Y})$ denote the vertical displacement at point D and vertical normal stress at point B of the plate, respectively. Two failure probabilities $Pr[u_2^D(\boldsymbol{Y}) > u_0]$ and $Pr[\sigma_{22}^B(\boldsymbol{Y}) > \sigma_0]$ are defined based on exceeding the displacement and stress thresholds $u_0$ and $\sigma_0$, respectively. Using SEFGM, Figs. 8 and 9 show the displacement-based failure probability $Pr[u_2^D(\boldsymbol{Y}) > u_0]$ and stress-based failure probability $Pr[\sigma_{22}^B(\boldsymbol{Y}) > \sigma_0]$ as functions of the corresponding thresholds for $\sigma_E = 0.12$ and 0.24 units, respectively. In both figures, the threshold values were
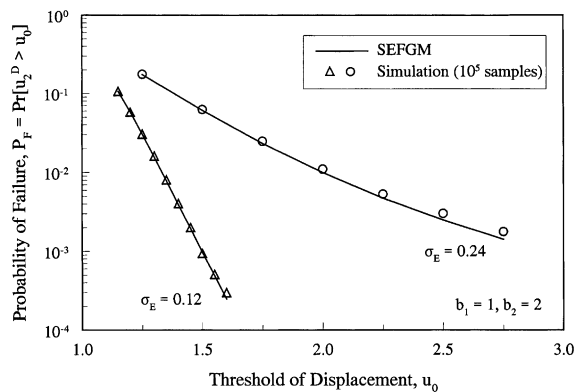


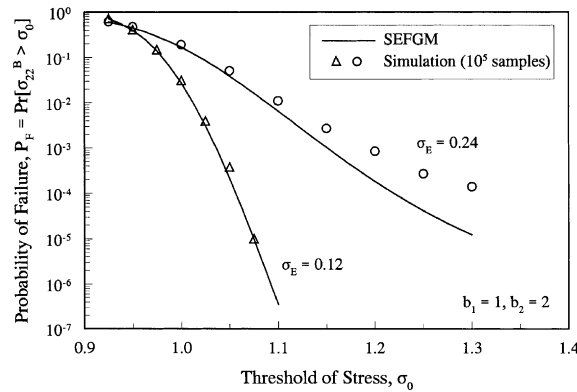Fig. 8. Displacement-based probability of failure of the plate.

Fig. 9. Stress-based probability of failure of the plate.

selected in a manner to yield "small" failure probability of interest. As before, the probability failure is larger for a large standard deviation of input. The results of Monte Carlo simulation using 100,000 samples are also given in Figs. 8 and 9. Good agreement is observed between the failure probabilities predicted by SEFGM (FORM) and simulation.

Fig. 10 shows how $Pr[u_2^D(Y) > u_0^*]$ varies as a function of the correlation length parameters $b_1$ and $b_2$ when $u_0^* = 1.35$ units and $\sigma_E = 0.12$ units. The probability of failure depends on both $b_1$, and $b_2$; however, the dependence on $b_2$ is stronger than on $b_1$, due to the vertical displacement considered. Otherwise, the results exhibit similar trends as the bar problem presented in Section 5.1.

To study the effects of the distribution of meshless nodes on the failure probability, two additional stochastic analyses were conducted for two different discretizations, as shown in Fig. 11(a) and (b). The total number of nodes is the same (i.e., $N = 49$) in both these discretizations, however, their nodes are irregularly distributed in comparison with the distribution in Fig. 7(b). Fig. 12 shows the plots of the failure probability, $Pr[u_2^D(Y) > u_0]$ vs. $u_0$, calculated using regular (Fig. 7(b)), irregular A (Fig. 11(a)), and irregular B (Fig. 11(b)) distributions of the meshless nodes. The same inputs defined earlier were used in all cases. According to Fig. 12, the failure probabilities due to all three discretizations are almost identical. No meaningful difference in the results is observed from irregularity in the meshless discretization. Note that the lack of sensitivity of the stochastic response to the nodal distribution is consistent with deterministic
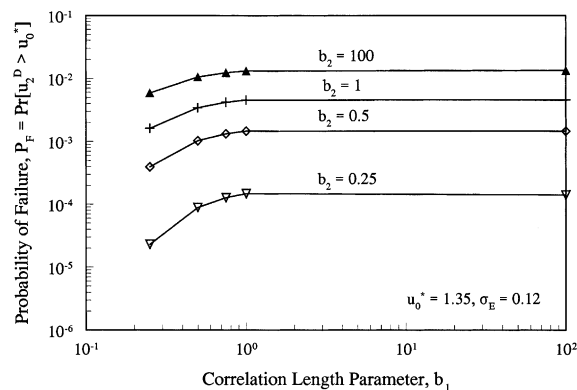


Fig. 10. Effect of correlation length on failure probability of the plate.

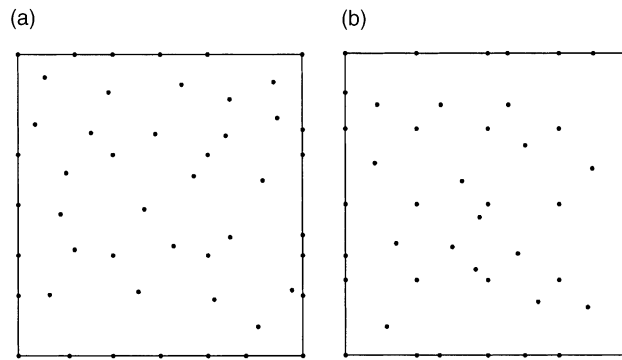(a)                                    (b)



Fig. 11. Irregular distribution of meshless nodes: (a) irregular A (49 nodes); (b) irregular B (49 nodes).
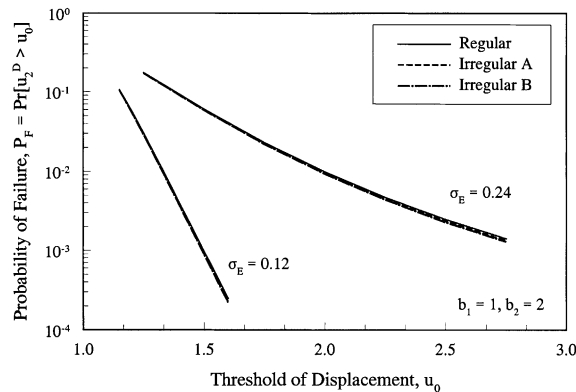


Fig. 12. Sensitivity of failure probability of the plate to nodal distribution.

observations made by some researchers in the field of meshless methods (Belytschko et al., 1994, 1995; Lu et al., 1994).

## 6. Conclusions

A SEFGM was developed for predicting probabilistic response and reliability of linear-elastic structures subject to spatially varying random material properties. The random field representing material properties was discretized into a set of random variables with their statistical properties obtained from the statistical properties of the random field. In conjunction with meshless equations, the FORM was employed to predict the full probabilistic characteristics of a structural response. Unlike the SFEM, the method developed herein requires no structured mesh, since only a scattered set of nodal points is required in the domain of interest. There is also no need for fixed connectivities between nodes. Numerical examples based on one- and two-dimensional problems have been presented to evaluate the accuracy and convergence of the failure probability by the developed meshless method. Good agreement is observed between the results of the developed method and Monte Carlo simulation. Furthermore, the stochastic meshless method provides convergent solutions of the probability of failure. Since mesh generation of complex structures can be a far

more time-consuming and costly effort than solution of a discrete set of equations, the developed meshless method provides an attractive alternative to FEMs in solving stochastic-mechanics problems.

## Acknowledgements

## References

Arora, J.S., 1989. Introduction to Optimum Design. McGraw-Hill, New York.

Belytschko, T., Lu, Y.Y., Gu, L., 1994. Element-free Galerkin methods. International Journal of Numerical Methods in Engineering 37, 229–256.

Belytschko, T., Lu, Y.Y., Gu, L., 1995. Crack propagation by element-free Galerkin methods. Engineering Fracture Mechanics 51 (2), 295–315.

Chen, J.S., Wang, H.P., 2000. New boundary condition treatments in meshfree computation of contact problems. Computer Methods in Applied Mechanics and Engineering 187 (3–4), 441–468.

Deodatis, G., 1991. Weighted integral method I: stochastic stiffness matrix. ASCE Journal of Engineering Mechanics 117 (8), 1851–1864.

Der Kiureghian, A., Liu, P.-L., 1986. Structural reliability under incomplete probability information. ASCE Journal of Engineering Mechanics 112 (1), 85–104.

Der Kiureghian, A., Ke, J.-B., 1988. The stochastic finite element method in structural reliability. Probabilistic Engineering Mechanics 3 (2), 83–91.

Duarte, C.A.M., Oden, J.T., 1996. H–p clouds—an h–p meshless method. Numerical Methods for Partial Differential Equations 12 (6), 673–705.

Ghanem, P.D., Spanos, P.D., 1991. Stochastic Finite Element: A Spectral Approach. Springer, New York.

IASSAR Subcommittee on Computational stochastic Structural Mechanics, 1997. A state-of-the-art report on computational stochastic mechanics. In: Schueller, G.I. (Ed.), Probabilistic Engineering Mechanics, vol. 12 (4). pp. 197–321.

Lancaster, P., Salkauskas, K., 1981. Surfaces generated by moving least squares methods. Mathematics of Computation 37, 141–158.

Li, C.-C., Der Kiureghian, A., 1992. Optimal discretization of random fields. ASCE Journal of Engineering Mechanics 119 (6), 1136–1154.

Libersky, L.D., Petschek, A.G., Carney, T.C., Hipp, J.R., Alliahdadi, F.Z., 1993. High strain Lagrangian hydrodynamics. Journal of Computational Physics 109, 67–75.

Lim, O.K., Arora, J.S., 1986. An active set RQP algorithm for optimum design. Computer Methods in Applied Mechanics and Engineering 57, 51–65.

Liu, W.K., Belytschko, T., Mani, A., 1986. Random fields finite element. International Journal for Numerical Methods in Engineering 23, 1831–1845.

Liu, W.K., Mani, A., Belytschko, T., 1987. Finite element methods in probabilistic mechanics. Probabilistic Engineering Mechanics 2 (4), 201–213.

Liu, W.K., Jun, S., Zhang, Y.F., 1995. Reproducing kernel particle methods. International Journal of Numerical Methods in Fluids 20, 1081–1106.

Liu, W.K., Li, S., Belytschko, T., 1997. Moving least square kernel Galerkin method. Part I: methodology and convergence. Computer Methods in Applied Mechanics and Engineering 143, 422–433.

Lu, Y.Y., Belytschko, T., Gu, L., 1994. A new implementation of the element free Galerkin method. Computer Methods in Applied Mechanics and Engineering 113, 397–414.

Lucy, L., 1977. A numerical approach to testing the fission hypothesis. Astronomy Journal 82, 1013–1024.

Madsen, H.O., Krenk, S., Lind, N.C., 1986. Methods of Structural Safety. Prentice-Hall, Englewood Cliffs, NJ.

Melenk, J.M., Babuska, I., 1996. The partition of unity finite element method: basic theory and applications. Computer Methods in Applied Mechanics and Engineering 139, 280–314.

Middleton, D., 1996. An Introduction to Statistical Communication Theory. IEEE Press, Piscataway, NJ.

Monaghan, J.J., 1988. An introduction to SPH. Computer Physics Communications 48, 89–96.

Nayroles, B., Touzot, G., Villon, P., 1992. Generalizing the finite element method: diffuse approximation and diffuse elements. Computational Mechanics 10, 307–318.

Rahman, S., Rao, B.N., 2001. A perturbation method for stochastic meshless analysis in elastostatics. International Journal for Numerical Methods in Engineering 50, 1969–1991.

Rahman, S., Xu, H., 2001. A meshfree method for computational stochastic mechanics. International Journal for Numerical Methods in Engineering, submitted for publication.

Rao, B.N., Rahman, S., 2000. An efficient meshless method for fracture analysis of cracks. Computational Mechanics 26, 398–408.

Spanos, P.D., Ghanem, R.G., 1989. Stochastic finite element expansion for random media. ASCE Journal of Engineering Mechanics 115 (5), 1035–1053.

Vanmarcke, E.H., Grigoriu, M., 1983. Stochastic finite element analysis of simple beams. ASCE Journal of Engineering Mechanics 109 (5), 1203–1214.

Yamazaki, F., Shinozuka, M., 1988. Neumann expansion for stochastic finite element analysis. ASCE Journal of Engineering Mechanics 114 (8), 1335–1354.

Zhang, J., Ellingwood, B., 1994. Orthogonal series expansions of random fields in reliability analysis. ASCE Journal of Engineering Mechanics 120 (12), 2660–2677.